

Electrical characterization of MeV heavy-ion-induced damage in silicon: Evidence for defect migration and clustering

P. K. Giri and Y. N. Mohapatra^{a)}

Department of Physics, Indian Institute of Technology, Kanpur 208016, India

(Received 1 December 1997; accepted for publication 29 April 1998)

We have studied electrical activity of defects created by high-dose MeV heavy-ion implantation in *n*-silicon. Heavy damage induced by Ar⁺ and Au⁺ ions is embedded within depletion layers of Schottky diodes. The defects are characterized using capacitance–voltage (*C–V*), current–voltage (*I–V*), deep-level transient spectroscopy (DLTS) and time analyzed transient spectroscopy techniques. Large concentration of defects in the depletion layer of as-implanted device lead to unusual features in *C–V* and *I–V* characteristics. The damage layer is found to extend several microns beyond the ion range or the damage profile predicted by standard Monte Carlo simulation packages. The dominance of a single trap in the damaged region is established from hysteresis effect in *C–V*, space-charge-limited conduction in forward *I–V* and DLTS spectrum. With annealing in the temperature range of 400–600 °C, the observed changes in the defect profile indicate that the effective electrical interface between damaged and undamaged layer moves progressively towards the surface. From transient spectroscopic analysis the major defect is found to be a midgap trap whose energy is sensitive to the degree of disorder in the damaged layer. The experimental features in *C–V* characteristics have been simulated using model charge profiles taking into account crossing of the Fermi level with the midgap trap within the depletion layer. The simulations suggest the presence of a compensated region and a sharp negatively charged defect profile at a distance much larger than that expected from ion range. Our results constitute experimental evidence, in qualitative agreement with recent predictions of molecular dynamics simulations, of defect migration and clustering of interstitial related defects even at room temperature in the case of high-dose irradiation. © 1998 American Institute of Physics. [S0021-8979(98)06115-5]

I. INTRODUCTION

There has been a recent thrust in studies of defects induced by high-dose irradiations of MeV heavy ions in semiconductors motivated by the increasing importance of such ion beams in processing technologies.^{1–3} At present, it is not clear as to which aspects and to what extent our understanding of light particles, low-energy, and low-dose implantation can be carried over to the cases of high-dose, high-energy, and heavy-ion implantations. There are likely to be significant differences in the nature of evolution of damage, distribution of defects, and their electrical manifestation in these different ranges of parameters. In spite of considerable progress in studies on implantation-induced damage, there is clearly two discernible limits of damage which have received most attention. At the lower limit of damage, only isolated point defects occur, which have been studied in great detail by techniques such as electron paramagnetic resonance and deep-level transient spectroscopy (DLTS).^{4,5} In the limit of high damage the focus has been on the formation and evolution of extended defects accessible to structural tools such as cross-sectional transmission electron microscopy.⁶ The intermediate regime of damage, though inaccessible to conventional probes, plays an important role in many phenomena of current interest such as defect clustering, transient enhanced diffusion,⁷ modification of properties of buried layers as in

rare-earth doping, etc.⁸ Recently, there has been simulational studies using molecular dynamics in this regime,^{9,10} though empirical studies for comparison are lacking. In a recent study, Benton *et al.*¹¹ have attempted to trace the evolution of damage induced by MeV Si ions in Si with dose and annealing in an effort to provide what they term as the “missing link” between point defect and extended defect regimes.

Electrical studies in the high damage regime have been meager, principally because they have been restricted to resistivity profiles,¹² and therefore, defects controlling compensation and trapping are the least understood. Studies involving the electrical characterization of point defects, particularly those involving depletion layer capacitance and transients, deliberately avoid complexities attributable to heavy damage in order to preserve the validity of the techniques used and the simplicity of interpretations. There is a strong need for attempts to extend the scope of such techniques, thereby identifying the electrical manifestation of defects distinct to the regime of heavy damage. We show here that such studies would be helpful in issues of recent concern in heavy-ion implantation such as long-range defect migration, disagreement between predicted and observed defect profiles, and evolution of defect clusters.^{11,13,14}

In this work, we have investigated the electrical manifestation of damage in MeV heavy-ion- (Ar⁺, Au⁺) implanted Si. Steady-state capacitance measurements have been carried out on Schottky diodes, with the damaged layer em-

^{a)}Electronic mail: ynm@iitk.ernet.in

bedded within the depletion layer, as a function of the voltage sweep rate, temperature, and annealing conditions. Unusual features in capacitance–voltage (C – V) and current–voltage (I – V) characteristics have been correlated with the defect-dominated nature of the damaged layers. Numerical simulations with model charge profiles are performed to reproduce the experimental features of C – V characteristics. Issues of defect migration and clustering have been discussed in view of these results. Transient spectroscopic methods, namely, deep-level transient spectroscopy and time analyzed transient spectroscopy (TATS) have been utilized to isolate the dominant defect in these materials.

II. EXPERIMENTAL DETAILS

A. Sample preparation

Epitaxial layers of phosphorous-doped n -Si with resistivity 2–5 Ω cm were used for this study. Vacuum annealed back Ohmic contacts were made on the n^+ substrate. The wafers were irradiated from the front side at room temperature using a 2 MeV Van de Graaff accelerator with Ar^+ ions at doses 5×10^{13} and 1×10^{14} cm^{-2} . These fluences are below the amorphization threshold of Ar^+ ions,¹⁵ and were chosen so as to create heavy damage typical of high-dose applications without causing amorphization. The beam current was chosen below microampere to avoid any significant heating of the sample during irradiations. A few samples irradiated with 4.6 MeV Au^+ ions at a dose of 5×10^9 cm^{-2} were also studied for comparison with Ar^+ ions. Schottky contacts were made by evaporating gold dots of 1 mm diam. The as-implanted samples did not receive any other high-temperature annealing except for heating at 70 $^\circ\text{C}$ for 30 min for curing the contact epoxy. A few finished devices having implant-induced damage were oven annealed at 160 $^\circ\text{C}$ for 30 min to study any possible damage relaxation. To monitor the effect of annealing, two groups of irradiated wafers were annealed in vacuum ($\approx 2 \times 10^{-6}$ Torr) for 30 min at 400 and 600 $^\circ\text{C}$ prior to Schottky contact formation.

B. Measurements

Capacitance measurements were done using a Boonton capacitance meter (model 72B) operated at 1 MHz. All transient measurements were carried out using an automated setup. Typically, in a C – V measurement, unless otherwise specifically mentioned the bias voltage is changed from high reverse bias to zero bias so that the time dependence of the trap occupancy does not affect the steady-state capacitance measurements. In DLTS measurements, at each temperature several transients (typically, ten) are acquired and averaged. DLTS signals corresponding to seven different rate windows are obtained enabling construction of Arrhenius plots from a single temperature scan.

TATS is an isothermal spectroscopic technique based on the sweeping rate window in the time domain, which is in contrast to DLTS where the rate window is kept fixed and the temperature is varied. TATS signal S is given by¹⁶

$$S(t) = C(t, T) - C(t + \gamma t, T), \quad (1)$$

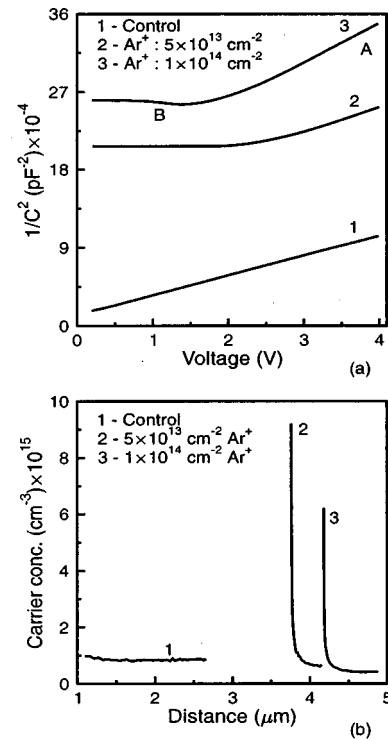


FIG. 1. (a) Typical C – V characteristics at $T = 300$ K for the n -Si Schottky diode before and after irradiation with various doses of Ar^+ ions. (b) Apparent carrier-concentration profile obtained from differentiation of curves of (a).

where C represents the isothermal capacitance transient at temperature T and γ is an experimentally selectable constant. $S(t)$ has a maximum at time t_m when plotted against $\ln(t)$. For an exponential transient of the time constant τ_e , t_m , and τ_e are related by

$$\tau_e = \frac{\gamma t_m}{\ln(1 + \gamma)}. \quad (2)$$

TATS being an isothermal spectroscopic technique, it has several advantages over DLTS, especially in the present case where the nature of transients is strongly temperature dependent. We have demonstrated its efficacy in studies of defect processes in the case of semi-insulating GaAs,¹⁷ DX centers in AlGaAs,¹⁸ and ion-induced defects in deep buried layers in Si.¹⁹ In a typical TATS measurement, transient data are acquired over 4 (1/2) orders of magnitude in time at a stabilized temperature. To avoid nonexponentiality due to high trap density, transient measurements were performed in constant capacitance mode where the voltage transient is monitored keeping the capacitance constant using a feedback circuit.²⁰

III. RESULTS

A. C – V characteristics

Figure 1(a) shows a typical $1/C^2$ versus V plot at room temperature for unimplanted and Ar^+ ion implanted samples with two different doses. It can be noted that for the unimplanted samples, the curve is linear in the measured voltage range indicating uniformity of shallow doping concentration.

However, for implanted samples there are distinctly two regions [marked A and B in Fig. 1(a)] of which the linear region A occurs for higher voltages and the flatter region B occurs for lower voltages. Since depletion width W is proportional to $1/C$, Fig. 1(a) clearly shows that zero bias (or, even for any particular applied bias) the depletion width systematically increases on increasing the dose of implantation. Similar qualitative features are observed for Au^+ -implanted silicon even though the doses used are only $5 \times 10^9 \text{ cm}^{-2}$.

Figure 1(b) shows the apparent free-carrier concentration versus depletion width W , which is obtained by differentiating the curves of Fig. 1(a) for the unimplanted and implanted samples. For the unimplanted samples, the carrier profile is seen to be uniform and the concentration is in accordance with the background doping of the epitaxial layers. For implanted samples, the apparent carrier profiles show a sharp rise for the lowest W corresponding to the flat region in the respective $C-V$ characteristics. It is known that the presence of deep acceptors with peaked profiles (as usual in implanted samples) cause artifactual peaks and dips in the carrier concentration profiles obtained from $C-V$.^{21,22} The nature of our observations, on the other hand, seem to be distinctly different in two respects. First, there is only a very sharp rise, and second, the depths at which these sharp rises occur are very large, i.e., at about four times the zero bias width of the control diodes in the case of Ar^+ -implanted Si. We go on to show that this feature in the carrier profile is an artifact due to a large trap density in the region of the depletion layer. However, the location of this trap-dominated region lies far beyond the range predicted by TRIM²³ (transport of ions in matter), which is only $1.23 \mu\text{m}$. A large concentration of traps is expected to be present in the as-implanted Si, but its location is unusual.

The flatness in the $C-V$ characteristic has been reported earlier in Mg^+ - and Ni^+ -implanted Si (Ref. 24) and in He ion-implanted Si (Refs. 25–27) without a discussion of its origin. Singh²⁸ has attributed the occurrence of such flat regions to interface states in $\text{Ni}/n\text{CdF}_2$ Schottky diodes using ideas suggested by Fonash.²⁹ High series resistance in the device can give rise to such features.³⁰ Consequently, this yields the wrong carrier-concentration profile. However, for our irradiated devices, independent measurement of the dissipation factor ($\omega R_s C$, where R_s is the series resistance and C is the actual capacitance) at various temperatures using an impedance analyzer showed no significant effect of series resistance in the capacitance measurement. The dissipation factor was found to vary in the range of 0–0.17, the larger value being for higher temperature, in the temperature range of 100–310 K. The series resistance effect becomes significant when the dissipation factor is comparable to or greater than 1. Moreover, it can be shown that large series resistance gives rise to a minima in the $1/C^2$ versus V curve rather than flatness as observed. Hence, this effect is a significant characteristic of the damaged region in the depletion width. We go on to present more parametric dependence on $C-V$ curves in order to isolate the origin of these features.

$C-V$ measurements were also carried out at various temperatures in the range 100–310 K. Figure 2 shows the $1/C^2$ versus V plot for low-dose Ar^+ ion irradiated Si mea-

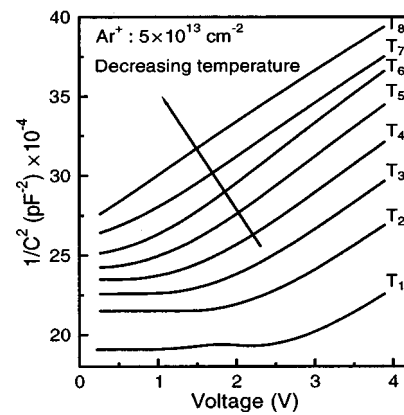


FIG. 2. $C-V$ characteristics of as-implanted n -Si measured at temperatures (T1) 303.9 K, (T2) 278.3 K, (T3) 257.4 K, (T4) 237.9 K, (T5) 217.2 K, (T6) 186.6 K, (T7) 155.5 K, and (T8) 103.5 K.

sured at various temperatures in the range 100–310 K. In these measurements, at a fixed temperature the sample is initially kept at steady-state reverse bias and then $C-V$ data are taken by changing the bias from high to low reverse bias. The change in capacitance with temperature is seen to be large, as shown in Fig. 2. Note that as the temperature is decreased from T_1 to T_8 in Fig. 2, the depletion layer edge for any particular bias (say, zero bias) lies deeper in the sample. Further, the extent of voltage of the flatter region gets reduced and the curves at the lowest temperatures are fully linear, indicating constancy of carrier concentration. These distinct features taken together point to the involvement of traps in controlling the nature of the curves. Large changes in capacitances, say at zero bias, are an indicator of changes in the charged trap occupancy within the depletion layer with temperature. Clearly, the trapped charge is such that the depletion width is large at lower temperature. For higher temperatures and lower voltages, the traps seem to affect the $C-V$ curve, their occupancy being controlled by crossing of the Fermi level with the trap level within the depletion layer. These systematics were observed in all our damaged samples. The increase in depletion width in the presence of the damaged region seems to be a consequence of the acceptor nature of the dominant traps in the damaged region. These interpretations are further supported by the hysteresis measurements described next.

The trap-dominated nature of the damaged layer is confirmed by observation of the hysteresis behavior in the $C-V$ measurement. Figure 3 shows $1/C^2$ versus V plots at a certain low temperature for different voltage sweep rates in both directions of voltage change. A typical scan begins with decreasing reverse voltage from a steady-state value. Note that the $C-V$ characteristics depend on both the rate and direction of the voltage sweep, clearly showing the hysteresis effect. The occurrence of hysteresis can be easily understood in terms of the presence of a large number of trapping centers in concentration comparable to or larger than the background doping. During $C-V$ measurement, if the voltage sweep rate is made faster/comparable to the trap emission rate, one observes a difference in capacitance between the decreasing and increasing voltage sweep. For the fastest sweep rate the

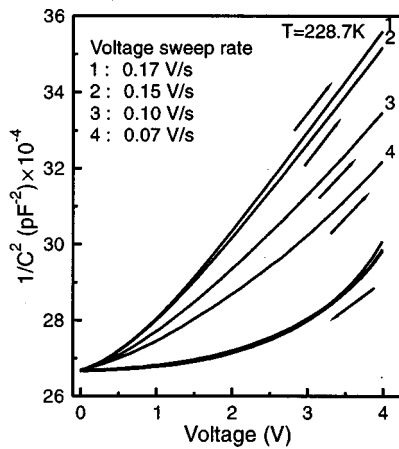


FIG. 3. $1/C^2$ vs V plot showing hysteresis behavior for decreasing and increasing reverse bias with different voltage sweep rates. Arrows indicate the direction of voltage sweep.

difference between the two curves are maximum and for the slow sweep rate the upper curve approaches the lower curve as shown in Fig. 3. It can be noted that the $C-V$ characteristics are identical for different sweep rates when the voltage is decreased owing to the fast capture process at the traps, while it is different when increasing the voltage since it is now controlled by the rate of emission. Thus, it is clear that the flat region or nonlinearity in $C-V$ is due to trap filling during decreasing reverse bias. From transient measurement data presented later, we find that the sweep rates used here are comparable to the emission rate of a single major trap identified in this work. The zero bias depletion width of most devices having damaged layers are 2–3 μm larger than their corresponding undamaged devices. Also, note that the depletion width is larger when the reverse bias is increased after allowing capture during $C-V$ measurements. This implies that after the capture of electrons, the defects become negatively charged in such a large number that the depletion region is widened to uncover the required amount of positive background charge to maintain the charge balance condition. Hence, these traps play the role of a dominant compensating center.

We have observed a similar hysteresis effect for Au^+ -implanted Si as well. In Fig. 4, we show that the hysteresis can be obtained by controlling the extent of filling of the traps by forward biasing the device, and keeping the sweep rate constant for different cycles. During the decreasing voltage cycle we take the device to forward bias, indicated as negative voltage in Fig. 4. The vertical arrows on the voltage axis in Fig. 4 indicate the voltage up to which the forward bias is applied before starting reversal of the direction of the sweep. With increasing forward bias, we see a larger hysteresis effect, i.e., the difference between the curves corresponding to the decreasing and increasing voltage cycle increases. The occurrence of negative slopes in these curves is indicative of the profile in the trap concentration. Consider, for example, the filling curve denoted by the solid line during the voltage change from reverse toward forward bias. Around zero bias, an increase in forward bias leads to such an increase in the negative trapped charge that

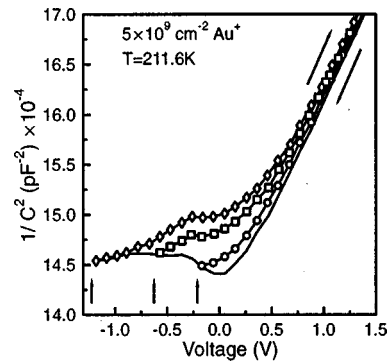


FIG. 4. $C-V$ characteristics with decreasing and increasing bias showing hysteresis effect in Au^+ -implanted n -Si. Slanted arrow indicates the direction of voltage sweep, and a different set of curves was obtained for different degrees of forward bias injection. The forward bias voltage for each is indicated by vertical arrows above the voltage axis.

the depletion width is forced to widen at the same bias to uncover the additional positive charge at the edge. Hence, the slopes are due to the combined effect of trap occupation in the depletion layer and dopant charges at the edge of the depletion layer.

The observation of hysteresis with different degrees of filling and various sweep rates establish that $C-V$ is controlled by large trap concentration due to irradiation damage in these samples. We go on to show their manifestation in $I-V$ measurements.

B. $I-V$ characteristics

In our irradiated devices, a major deviation from conventional $I-V$ characteristics of the Schottky barrier (our control diode) occurs due to the presence of a damaged layer. Such behavior is seen in both Ar^+ and Au^+ irradiated devices.

For the Ar^+ irradiated device, both forward and reverse currents are significantly smaller compared to the corresponding currents in the unirradiated device. This is indicative of the presence of a compensating region in the depletion region of the device. For voltages corresponding to low forward bias, the magnitude of the current is low enough for unproblematic capacitance measurements. However, there is a sudden jump of current for certain forward voltage in the irradiated devices. In Fig. 5, we have plotted $I-V$ curves in a log-log scale measured at three different temperatures for an Ar^+ ion-implanted sample annealed at a low temperature (160 $^\circ\text{C}$ for 30 min). Each curve shows a near-ideal case of crossover from Ohmic conduction ($I \propto V$) to the square-law space-charge-limited conduction ($I \propto V^2$) regime at the voltage corresponding to the trap filled limit (V_{TFL}). The nearly vertical rise in current accompanying the trap filling is an indicator that the associated trap is a discrete level.³¹ The same defect controls hysteresis in $C-V$ measurements due to its large concentration, and is responsible for the near-intrinsic behavior of the damaged region. Thus, the structure under study is akin to the $p-i-n$ diode where p is replaced by a metal and the i region is nearly intrinsic due to the above defect level. Similar results of space-charge-limited

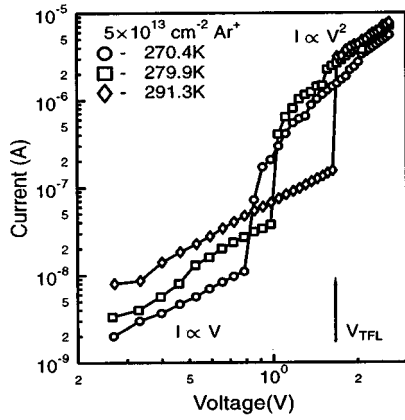


FIG. 5. Forward I - V characteristics of a 160 °C annealed sample at different temperatures showing Ohmic and space-charge-limited (SCL) current regions. Shift in trap filled limit voltage (V_{TFL}) can be seen for different temperatures.

conduction have been reported for silicon amorphized by ion implantation,³² and for proton bombarded GaAs.³³

The notable feature in this set of curves is the decrease of V_{TFL} with decreasing temperature. The observed shift of V_{TFL} can be explained on the basis of trap filling with lowering temperature at a fixed bias. As the Fermi level moves closer to the conduction band in n -Si upon reduction in temperature, more traps get filled. Thus, the number of the unfilled fraction reduces with the lowering temperature, decreasing in turn the V_{TFL} .

An unambiguous observation of space-charge-limited current proves the presence of a fully trap-controlled region in the depletion region of the irradiated diode. Space-charge-limited current measurements have been used in the literature to determine the energetic distribution and spatial profile of bulk traps in semiconductors.^{31,34} However, in this case, accurate determination of the energetic distribution of traps or the trap profile from I - V characteristics is rendered difficult due to the nonuniform spatial distribution of the trap and temperature dependence of occupancy. Nevertheless, for purposes of a rough estimation of trap concentration, under the assumption of uniform trap distribution over most of the depletion layer, we can use the following equation:³¹

$$N_T = \frac{1.1 \times 10^6 \kappa V_{TFL}}{L^2} \text{ cm}^{-3}. \quad (3)$$

For $V_{TFL} = 1.7$ V (Fig. 5), the estimated trap density is $N_T = 5.5 \times 10^{14}$ cm^{-3} for a layer width of 2 μm . It is to be noted that the V_{TFL} measures that fraction of the total trap that is empty in thermal equilibrium. Moreover, the effective length over which trapping and detrapping occurs during the bias change is quite small compared to the total depletion width. Thus, the trap concentration peak value is much larger than the value estimated above. For our purposes, it suffices to note that a very large concentration of traps occurs within the depletion layer, controlling both its I - V and C - V characteristics.

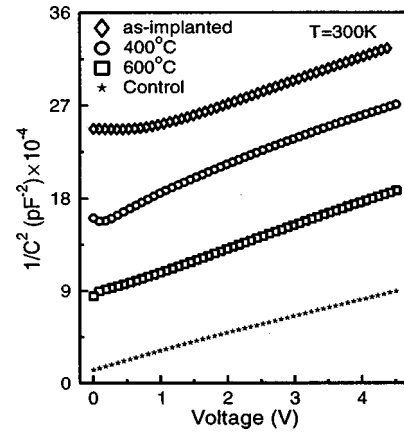


FIG. 6. Comparison of C - V characteristics at 300 K of unimplanted, as-implanted, and annealed n -Si implanted with 5×10^{13} cm^{-2} Ar^+ ions.

C. Effect of annealing on C - V and I - V characteristics

Figure 6 shows the $1/C^2$ versus V plot for Ar^+ ion irradiated n -Si before and after high-temperature annealing. We have justified previously the cause of the large depletion width in as-implanted devices. It is clearly seen that high-temperature annealing decreases the trap concentration. This leads to systematic changes in both the major features in the $1/C^2$ versus V curve. With an increase in annealing temperature, (i) the zero bias depletion width recovers towards the control samples, and (ii) the flat region for low bias reduces progressively. The temperature range of annealing (400–600 °C) itself suggests that the dominant defects controlling electrical behavior are point defects, since extended defects begin annealing out only at temperatures above 1000 °C. Comparison with unimplanted devices shows that 600 °C is not sufficient to remove all the defects completely as the depletion width for the implanted samples is larger than the unimplanted case. The near-parallel nature of the curves in Fig. 6 for the high reverse bias region indicates an absence of defects in the deeper region. For 400 °C annealed samples, we could observe the hysteresis effect in C - V measurements at room temperature. It was obtained for the fast sweep of voltage during decreasing and increasing bias voltage. This is also indicative of the changed time constant of the dominant defects controlling hysteresis. This has been confirmed from transient measurements as well.

Figure 7 shows a comparison of I - V characteristics at 300 K for samples annealed at 400 and 600 °C after implantation. The reverse saturation current is similar for these two samples. But, the forward characteristics of the 600 °C annealed samples is considerably improved as compared to the case of the 400 °C annealed samples. For the latter case, the space-charge-limited current above the trap filled limit voltage is clearly seen. Though V_{TFL} is not as large as it was for the as-implanted sample, the presence of a still larger trap concentration is clear. It is expected that these defects can be annealed out by annealing above 600 °C. These defects are anticipated to be due to point defect complexes or clusters rather than extended defects whose formation requires heat treatment at higher temperature.

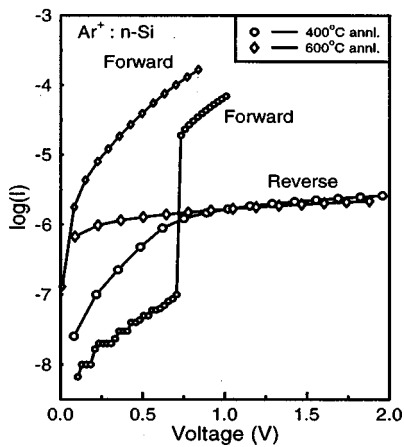


FIG. 7. Forward and reverse $I-V$ characteristics of Ar^+ -implanted samples after 400 and 600 °C annealing.

D. Transient spectroscopic studies

A typical set of DLTS spectra for samples irradiated with two different doses of Ar^+ ions and low-dose Au^+ ions are shown in Fig. 8(a); the evolution of DLTS spectrum for a particular sample with oven annealing at a relatively low temperature of 160 °C is shown in Fig. 8(b). Two majority-carrier related peaks labeled V_2 and D1 are observed in the spectra irrespective of ion species and dose. The peak labeled

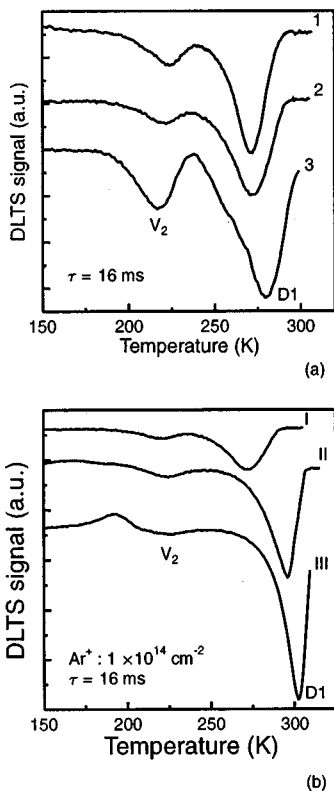


FIG. 8. (a) A set of typical DLTS spectra for (1) $5 \times 10^{13} \text{ cm}^{-2} \text{ Ar}^+$ ions, (2) $1 \times 10^{14} \text{ cm}^{-2} \text{ Ar}^+$ ions, and (3) $5 \times 10^9 \text{ cm}^{-2} \text{ Au}^+$ ions irradiated n -Si. Two peaks V_2 and D1 are common in all spectra. (b) A set of DLTS spectra for (I) as-implanted, (II) 160 °C, 30 min annealed, and (III) 160 °C, 3 h annealed samples implanted with high-dose Ar^+ ions.

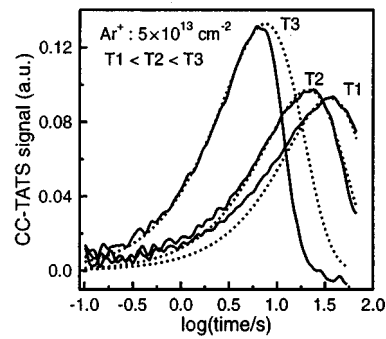


FIG. 9. CC-TATS spectra (solid line) of D1 measured at temperatures (T1) 212.7 K, (T2) 217.7 K, and (T3) 228.6 K. The dotted line corresponds to the peak fitted with exponential transients showing broad, exponential, and narrow peaks, respectively.

V_2 is due to the second ionization of the well-known divacancy center at energy $E_c - 0.42 \text{ eV}$ with a capture cross-section of $3 \times 10^{-15} \text{ cm}^2$. This is in good agreement with the reported values in the literature.^{5,35,36} The observed concentration of this defect is smaller than expected, most probably due to suppression of its formation by more efficient defect reactions in the case of high-dose irradiations. The peak labeled as D1 is a newly found level, which occurs consistently in a large concentration in our samples implanted with high doses. The emission rate of defect D1 for a particular temperature as obtained from DLTS spectra and the sweep rate of the voltage in hysteresis at the same temperature are comparable. Thus, the peak D1 related defect is the dominant trap controlling hysteresis in $C-V$ and space-charge-limited conduction in forward $I-V$ characteristics. To the best of our knowledge, this level has not been observed mostly because, to our knowledge, no other DLTS study uses unannealed samples with as high doses as in our case.

A comparison of spectra corresponding to unannealed and oven annealed samples [as depicted in Fig. 8(b)] shows several interesting features. With annealing, though the V_2 related peak height seems to have been reduced without any change of peak position, the D1 peak is shifted towards higher temperatures along with an increase in peak height. Also, note that this peak shape is substantially narrow, i.e., skewed at the right side compared to the as-implanted case. The shift in peak position in DLTS spectra implies that low-temperature annealing of the damaged layer results in deepening in emission energy of the dominant defect. Proper inspection of the transient causing the skewed peak in DLTS spectra reveals that it is due to premature termination of the transient.³⁷ Due to the occurrence of a cusplike peak in DLTS, and since a large concentration of defects are involved, conventional analysis to obtain the trap parameter for defect D1 is not appropriate.

In order to obtain reliable information regarding defect D1, an isothermal spectroscopic technique such as TATS in constant capacitance (CC) mode is employed. TATS signals corresponding to D1 at three different temperatures are shown in Fig. 9, where the dotted lines refer to fitted peaks corresponding to exponential transients in each case. For high temperature (T3), the TATS peak is seen to be narrower

than the exponential case. This is due to a change in the quasi-Fermi level during trap emission.³⁷ However, at lower temperatures this effect weakens due to less change in trap occupancy. At sufficiently low temperatures (as at T1), TATS peaks are found to be broader than corresponding exponential transients. Broadening in the line shape indicates distribution in emission energy. If a Gaussian distribution around the mean energy is assumed, energy broadening is about 25 meV for high-dose (Ar⁺) implanted Si, whereas it is only 6 meV for the low-dose Ar⁺-implanted sample. This broadening in energy can be attributed to lattice strain around the defect in the damaged layer. We have recently shown³⁷ that a careful analysis of the line shape of the TATS peak is necessary to obtain trap parameters in the presence of unusual sources of narrowness. It has been found that, depending on the dose and annealing conditions, the Arrhenius plot for the major peak yields an activation energy in the range 0.49–0.56 eV and an approximate capture cross section of 1×10^{-15} cm². The magnitude of the capture cross section is typical of a deep neutral center³⁸ accepting an electron to become negatively charged. The sensitivity of activation energy to annealing conditions and dose indicate the marked influence of changes in the environment of the defect in the damaged layer due to accumulation of disorder or relaxation. Thus, this defect can act as a probe in the study of the degree of disorder for high-dose implantations. In spite of moderate broadening, peak D1 has a point-defect-like line shape and corresponds to a well-defined defect. The fact that it occurs in high-dose irradiated samples, and does so prior to any high-temperature annealing, suggests that it is due to defect clusters.

IV. DISCUSSION

A. Qualitative explanation of major features in $C-V$

Let us first consider flatness in the low-bias regime of $C-V$ curves or the bias independence of the capacitance and the consequent nonlinearity of the $1/C^2$ versus V curves. It is well known that a trap can be occupied in the transition region of the depletion layer where the trap level is below the Fermi level. Let us consider an energy band for a Schottky diode with one uniformly distributed deep level at energy E_T , which becomes negatively charged when occupied with electrons. Changes in occupancy occur within the depletion layer at the location where E_F and E_T cross each other due to band bending. In our case, we are dealing with a large concentration and nonuniform spatial distribution of traps. It is worth mentioning here that in standard cases of small trap concentration, band bending is mainly controlled by background shallow dopants. For the present case, in contrast, trap concentration is so large that it controls band bending in the region of its presence, which in turn determines the crossing between E_T and E_F . Therefore, the location of the crossing is determined by the dynamics of the defect occupation. In the case of a depletion layer without deep traps, voltage changes across the device are accommodated through changes at the depletion layer edge. However, in the case of large trap concentration, changes of occupancy at the E_T-E_F crossing would control the total depletion width.

This process is responsible for nonexponential transients giving rise to narrow peaks in DLTS or TATS spectra.

From the experimental results it is clear that the occupied dominant traps produce charges opposite in sign to the background doping, i.e., they become negatively charged after capture of electrons. Hence, when reverse bias is increased (from, say, zero bias) the extra voltage drop can be accommodated either by increasing the depletion width, which leads to uncovering of positive charges at the edge, or by emitting electrons from the traps thereby increasing the net effective positive charge in the depletion layer. The former process would occur within the time constant of dielectric relaxation time while the later would be controlled by the trap emission rate. At sufficiently high temperature, if the trap emission rate is faster than the voltage sweep rate, detrapping at the crossing would itself accommodate the voltage change. The width of the depletion layer, and hence, capacitance would remain constant even when the bias is being changed, causing the feature of flatness. For larger biases, the trap concentration may not be sufficient to do so and the width would also increase in part. This would continue until the Fermi level loses contact with the trap level. Beyond this, the $C-V$ would reflect the background concentration giving rise to conventional linearity in the $1/C^2$ versus V curve. In this sense, the E_T-E_F crossing is the primary determinant in studies involving high-dose-implanted samples, while it is only a minor irritant in conventional depletion capacitance studies.

This explanation of major features in $C-V$ characteristics is fully consistent with the occurrence of hysteresis and temperature dependence. Hysteresis arises from the fact that the traps become occupied by a fast capture process at the crossing point during the decreasing bias cycle while on the increasing cycle the capacitance change is dependent on the slower emission process from the traps. Similarly, when temperature is decreased the bulk Fermi level of the semiconductor moves up in relation to the metal Fermi level causing the crossing point to move towards the surface. This leads to increased occupation of the traps; hence, increased negative charge forces the depletion layer to move out. At low temperature the traps filled in the process stay occupied, leading to both a larger zero bias depletion width, and linear $1/C^2$ versus V curves.

Therefore, information regarding electrically active defects would be from the E_T-E_F crossing point. In principle, by manipulating this crossing point in space, one can obtain charge profile information. However, the problem of identifying the absolute location in space where this crossing occurs is not straightforward. The measurement of capacitance only gives the location of the edge of the depletion layer and the crossing point relative to this edge would depend on the details of the profile inside. We have shown that the change of slope from the flat region to the linear region in $1/C^2$ versus V curves is rather sharp as represented in the apparent concentration profile [Fig. 1(b)]. The trap concentration profile at the crossing point is very sharp and can be treated as an "effective electrical interface" between trap-free and trap-dominated regions of the sample. The nature of this crossing point is distinctly different from that of a hetero-

junction or insulator–semiconductor interface capable of inversion. We have in the course of our work ruled out these possibilities on the basis of $C-V$ studies over an extended region of bias. Note that the doses used were below the amorphization threshold and it was several orders of magnitude lower in the case of Au^+ ion implantation. Yet, the nature of the characteristics are similar.

The deactivation of shallow dopants due to damage and charges due to electrically active traps produce a compensated region with low net charge density. The degree of compensation would be expected to have a profile more or less similar to the damage distribution as obtained from TRIM simulations.

B. Model simulations of $C-V$ characteristics

The purpose of model simulations is to arrive at the essential requirements of the charge profile that would reproduce the major features of $C-V$ characteristics. We seek to obtain reasonable estimates of the concentration of charges and the distances at which they are located without attempting to provide a numerical fit to the experimental data.

Several simplifying assumptions are required in order to keep the results of the simulation transparent. To account for the presence of the dominant trap indicated in the experiments, we assume that there exists only one midgap deep acceptor trap due to damage. The fact that its energy is in the middle of the band gap is justified on the basis of spectroscopic measurements. The region of the depletion layer from the surface to the location of the damage-induced trap is assumed to be uniformly compensated, having a low charge density. In reality, the degree of compensation would vary over distance with a profile more or less similar to that predicted for damage distribution. Compensation would mainly be due to deactivation of shallow dopants and the presence of deep defects in the region. However, the edge of the depletion layer is unable to penetrate into this layer during our capacitance measurements, preventing changes in the charge distribution in that region. Therefore, an assumed effective compensation would suffice to take into account the voltage drop across this region. We also assume that the metal–semiconductor barrier height is the same as that for control samples (i.e., a standard value of 0.8 eV for Au on the n -Si Schottky). This value only appears as a constant in the magnitude of voltage.

The one-dimensional Poisson equation is solved numerically for a particular choice of trap profile to obtain the band bending in the semiconductor. The voltage dependence of capacitance is obtained by integrating over different widths of the depletion layer. The trap occupation, band bending, and carrier concentrations are determined *self-consistently* during numerical integration. For the purposes of trap occupation, the Fermi occupancy function is replaced with the usual step approximation, i.e., all traps lying below the Fermi level are considered to be occupied, giving rise to a step in the occupancy at the $E_T - E_F$ crossing point. Nondegenerate carrier statistics were only needed for all simulations. The depletion approximation was not explicitly assumed, though

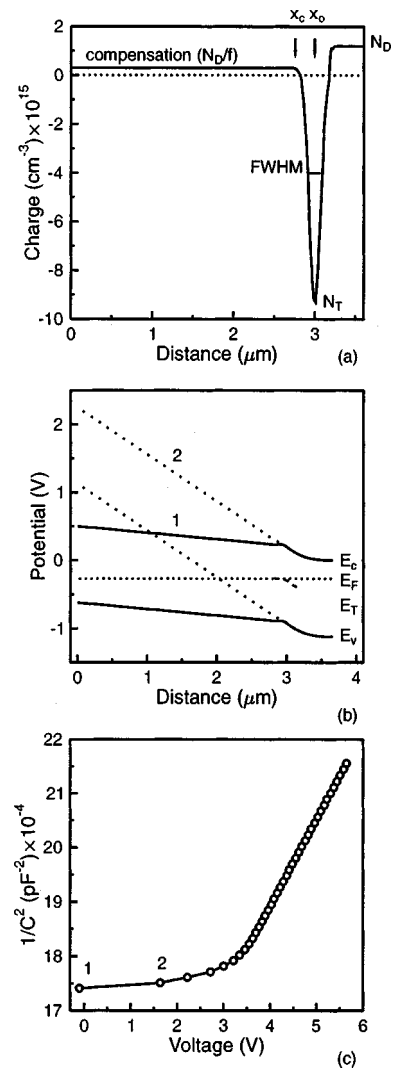


FIG. 10. (a) Typical charge profile due to trap concentration N_T and background doping N_D showing different parameters used for simulations. (b) Calculated energy-band diagram and (c) corresponding simulated $C-V$ characteristics for a Schottky diode with one acceptor trap level at energy E_T . Two sets of energy-band diagrams are shown corresponding to cases when: (1) all traps in the distribution are occupied, and (2) only a portion of the charge profile is occupied.

most of the results reported are well within the ambit of this approximation.

The parameters of simulation are specified in terms of a charge profile as depicted in Fig. 10(a). The relevant parameters are (i) the mean position (x_0) of trap profile (assumed to be Gaussian), (ii) the full width at half maximum (FWHM) ($2\sqrt{2} \ln 2 \sigma$, where σ is the standard deviation) of the Gaussian distribution, (iii) the maximum concentration of trap N_T , and (iv) the width of the compensated layer (x_c) and the level of compensation specified in terms of the fraction (f) of background doping (N_D). The Poisson equation can now be written as

$$\frac{d^2V}{dx^2} = -\frac{\rho_t + \rho_d}{\epsilon}, \quad (4)$$

where the trap charge density (ρ_t) and shallow donor density (ρ_d) are given by

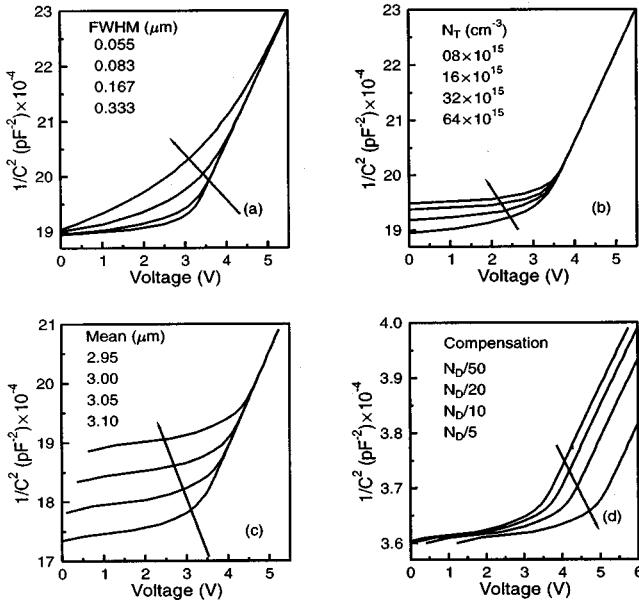


FIG. 11. Different parameter dependence of simulated $C-V$ characteristics for a Schottky diode with one acceptor trap level at energy E_T . The charge profile parameters are shown in Fig. 10(a) with parameters being varied as shown in each case: (a) FWHM of Gaussian distribution, (b) trap concentration (N_T), (c) mean of trap profile (x_0), and (d) compensation (N_d/f).

$$\rho_t = -qN_T \exp\left[-\frac{(x-x_0)^2}{2\sigma^2}\right],$$

$$\rho_d = \begin{cases} qN_d/f, & x < x_c \\ qN_d, & x > x_c \end{cases}$$

The simulations were tested using various standard cases of known trap and doping profiles. It correctly predicts, as expected from the analysis of Kimerling,²¹ the presence of artifactual peaks and dips in the apparent carrier concentration due to the presence of peaked profiles of deep acceptors. Typical results of a simulation corresponding to our case are shown in Figs. 10(b) and 10(c) where the energy band diagram and the resulting $1/C^2$ versus V are depicted in sequence. For a small change in depletion width w (first two points in the $C-V$ plot), the large change in band bending is shown due to the presence of a high trap density. The $C-V$ characteristics shown reproduced the major features of the experimental curves. The trap concentration and location are adjusted to obtain capacitance and voltage close to the experiments. Recall that the flatness in the $C-V$ curve is due to the fact that changes in trap occupation account for the extra voltage drop without necessitating significant changes in the depletion width as shown for points 1 and 2 in Fig. 10(c).

In order to evaluate how the choice of parameters affect the calculated $C-V$ curves, we have performed simulations varying each parameter at a time holding others constant. Figures 11(a)–11(d) show the sets of $C-V$ characteristics which clearly display different dependences. They can be summarized as follows:

(i) The sharpness of the transition from the flat to linear region is controlled by the FWHM of the trap distribution [Fig. 11(a)].

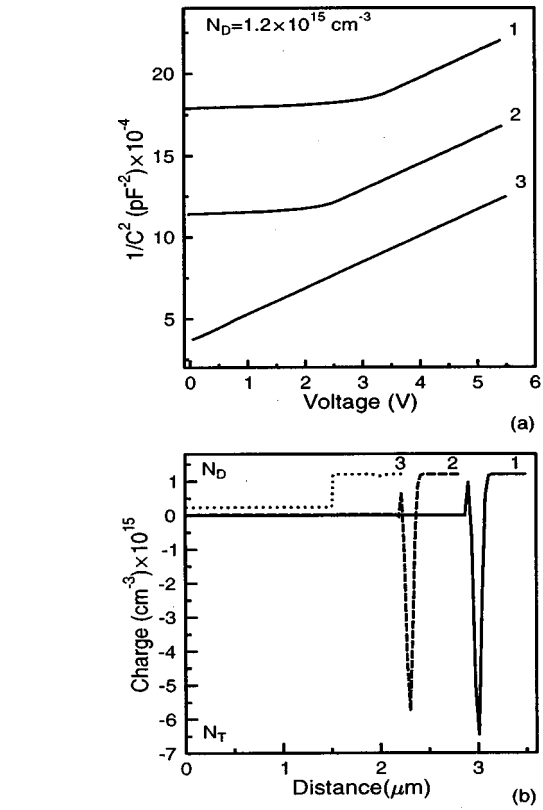


FIG. 12. (a) Simulated $C-V$ characteristics to reproduce the features due to different irradiation doses. (b) The corresponding charge profile. Compensation assumed for different cases were: (1) $N_d/5000$, (2) $N_d/50$, and (3) $N_d/5$.

(ii) The zero bias width is relatively insensitive to changes in trap concentration [Fig. 11(b)] but very sensitive to the choice of its mean position [Fig. 11(c)]. The mean position largely controls the level of capacitance of the flat region without affecting the linear portion.

(iii) The mean position of the trap profile strongly affects the zero bias depletion width [Fig. 11(c)].

(iv) The choice of the degree of compensation controls the linear shift of the characteristics along the voltage axis leaving the magnitude of the flat level capacitance unchanged [Fig. 11(d)].

The demonstration of the one-to-one relationship between the parameters and features in $C-V$ characteristics makes interpretation of experimental curves relatively straightforward, enabling us to fix parameters with confidence.

Figure 12(a) shows a set of $1/C^2$ versus V curves calculated to mimic the irradiation dose dependence as in the experimental curves of Fig. 1(a). The corresponding charge distribution (as distinct from the trap distribution) is shown in Fig. 12(b). The charge profile used to simulate them is consistent with the conclusions drawn from the experiments. For example, it supports the conclusions regarding gradual movement of the trap profile and compensation with variations in dose or annealing. Note that the required trap concentration is extremely high as compared to background doping.

The occupation profile of the traps accessible to our ex-

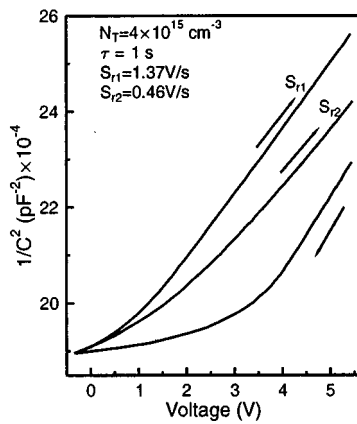


FIG. 13. Simulated $C-V$ curves showing hysteresis effect assuming a fixed rate of emission from one acceptor trap level at energy E_T .

periments is only the farther tail of the profile. Hence, we can only conclude that the trap concentration falls sharply towards the edge of the depletion layer. The assumption of a Gaussian distribution is only incidental and a means of providing an adjustable charge distribution corresponding to occupied traps. The occupied trap profile could as well have been assumed to be a narrow rectangular slice of charge at the E_T-E_F crossing. The idea of treating this crossing point as an “effective electrical interface” as introduced previously, gets reinforced through these simulations. The fraction of the depletion layer beyond this interface is only about $0.8 \mu\text{m}$, a value determined by the distance over which the voltage equivalent of (E_T-E_F) is dropped due to background dopant charges alone. Hence, most of the depletion width constitutes the region between the surface and the effective electrical interface. Changes in zero bias depletion width or the flat-region capacitance level with process variables such as irradiation dose and annealing temperature can, therefore, be traced to movement of this interface.

To be able to replicate the feature of hysteresis of $C-V$, we introduce a time constant of emission of the carrier from the trap into the simulations. A typical set of calculated curves demonstrating hysteresis in close agreement with experiment is shown in Fig. 13.

C. Physical processes: Defect migration and clustering

Armed with insights from simulation, we are now in a position to discuss the most perplexing aspect of the results. It has been mentioned that except for the last fraction of a micron, the depletion width is mostly due to the distance of the falling edge of the trap profile. The typical depletion width in samples containing damage is between 2.5 and $4 \mu\text{m}$. In contrast, the prediction of TRIM simulations give an end-of-ion range of $1.23 \mu\text{m}$ only. Hence, the question arises as to why the trap profile extends so much beyond the location of the end-of-ion range damage. There is also the related question of how is one able to change the interface between the trap-dominated and trap-free region through irradiation dose and annealing.

Any residual channeling in spite of misorientation of the surface with respect to the beam cannot lead to observation of a huge concentration of traps so far away from the location of the nuclear damage. This has been confirmed in another set of experiments,²⁷ in which n -Si samples were implanted with a very high dose of 1.5 MeV He ions at an angle as large as 60° to the surface normal so as to keep the range of these light ions to approximately $1-1.5 \mu\text{m}$. In these experiments also the total depletion width turned out to be larger than that predicted from TRIM simulations.

We propose that the dominant compensating deep acceptor traps have their origin in species which can migrate over large distances from the source of their creation even at room temperature. As migration occurs, these species would tend to form clusters rendering them immobile. This process of migration and cluster/complex formation can indeed lead to a profile with a sharply falling edge moving deeper into the sample.

The pieces of supporting evidence for such a mechanism are increasing in recently reported experimental and theoretical studies. Recently, Privitera *et al.*¹⁴ demonstrated room-temperature migration of Si interstitials over several microns. In these experiments interstitials generated at the surface migrated deeper into the sample to interact with pre-existing damage-induced defects.³⁹ Similarly, Larsen *et al.*,⁴⁰ in a study of migration of Si self-interstitials at room temperature using a spreading resistance technique, detected dopant deactivation up to a depth of several microns beyond the region directly modified by the ions. High fluence MeV implants, specifically with heavy ions, have usually been reported to result in a very wide spatial distribution of defects ($2-4 \mu\text{m}$) in contrast to TRIM predictions of a FWHM of only a fraction of a micron.^{13,14}

Jaraiz *et al.*⁹ have recently reported a set of significant results from molecular dynamic simulational studies of combined processes of defect generation, migration, and clustering during and after implantation. Their atomistic simulation show migration of free interstitials and clustering at room temperature even several hours after initial fast recombination processes have died out. They also show that the depth distribution of remnant interstitials peak at approximately twice the implant range. Defect clustering is known to be more favorable in heavy-ion irradiation due to the occurrence of a high density of collisional cascades in comparison to light ions. Similar effects are also expected for high-dose implants.¹¹ Therefore, there is a growing body of evidence showing that ion-induced damage acts as a source of migrating interstitials, which can combine to form clusters at distances beyond the damage location. Though the electrical activity of *point* defects and *extended* defects in implanted material have been studied in detail, there is a lack of similar studies on *defect clusters*. Only recently Benton *et al.*¹¹ have reported electrically active traps associated with second- and higher-order interstitial clusters in residual damage of Si implanted with high fluences. It appears reasonable to conclude that the dominant electrically active traps observed in our experiments also originate from interstitial clusters. The cluster binding energy is known to change with the size of clusters and this might be reflected in the activation energy

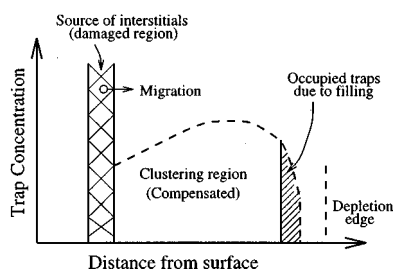


FIG. 14. Schematic diagram of the trap profile due to MeV heavy-ion implantation. The discontinuous line refers to the evolved trap profile due to migrating interstitials from the end-of-range damaged region (crossed lines). The shaded region on the right side shows the accessible (occupied) trap profile due to filling pulse.

of the associated defect. The sharp trap profile at distances much larger than ion range would be fully consistent with the mechanism of migration and eventual cluster formation of interstitials. Thus, our results constitute direct experimental evidence of such a mechanism.

Piecing together the results presented here along with the evidence of others, the view that emerges is summarized in a schematic sketch in Fig. 14. The region directly damaged by high doses of implanted species serve as a rich source of interstitials, which migrate deeper into the sample. They participate in formation of clusters enroute, thus leading to a large trap-dominated region beyond the range of the implanted ions. The trap concentration at the edge of the profile is so large and falls so sharply that it serves as a blocking wall in $C-V$ profiling experiments. The trap profile indicated by the discontinuous line to the left of the edge is not accessible to $C-V$ experiments through changes in occupation, and hence, do not contribute to the charge. The shaded region in the trap profile constitutes the occupied trapped charge, and hence, delineates the “effective electrical interface.”

The fact that the effective electrical interface moves with changes in the process variables, such as dose and annealing, also supports the occurrence of a mechanism involving migration and clustering. With an increase in irradiation dose, the interface between the trap-dominated and trap-free regions is expected to move deeper into the sample as there would be a more abundant supply of interstitials from the damaged region. Similarly, the effective interface is observed to move towards the surface with an increase in annealing temperature. Though the mechanism of recovery is unclear at this stage, it is most probably due to spatial variation of the degree of clustering. It is known that the binding energy for interstitial clusters increases with cluster size given by $E_{bi}(n) = 2.1 - 1.45(\sqrt{n} - \sqrt{n-1})$, where n is the number of interstitials in the cluster.⁹ Hence, a higher temperature is needed to repair regions containing larger clusters which are closer to the damage.

The origin of the D1 defect most probably lies in the formation of interstitial clusters. The sensitivity of carrier activation energy to processing conditions is also an indication in this direction. It is not clear why a single type of defect should dominate the spectra instead of producing a series of discrete levels or a continuum of energy levels cor-

responding to the distribution in cluster sizes. Our results point to the urgent need of obtaining a correlation between the electrical signatures of traps and the evolution of clustering in very high-dose-implanted samples. Though more detailed studies are required to pin down the mechanisms, our work demonstrates that capacitance-based studies can serve as an important tool in such an endeavor.

V. SUMMARY AND CONCLUSIONS

The role of electrically active defects in heavy-ion implantation-induced damage in silicon has been studied using capacitance-based techniques. It has been shown that characteristic features such as the occurrence of a bias-independent capacitance region, hysteresis, strong temperature dependence of capacitance, and space-charge-limited conduction are controlled by a large concentration of a dominant deep acceptor trap within the depletion layer. The effective electrical interface between the trap-free and trap-dominated regions is formed at the crossing between the trap level and Fermi level. Model simulations of $C-V$ characteristics were carried out to explain major features and to obtain the essential nature of net charge profiles. A sharp trap profile is seen much beyond the ion range and its location is found to be dependent on irradiation dose and annealing temperature. The observation of a sharp profile of traps at large distances has been explained on the basis of interstitial migration and clustering. Transient spectroscopic measurements show a dominant midgap defect, whose origin is attributed to interstitial cluster formation in high-dose-implanted silicon.

ACKNOWLEDGMENTS

The authors gratefully acknowledge the invaluable help provided by Dr. V. N. Kulkarni, Dr. Sankar Dhar, and T. Som in sample fabrication including ion irradiation. The authors are thankful to Dr. B. N. Dev and B. Sundaravel of the Institute of Physics, Bhubaneswar for their help in gold ion irradiations.

- ¹E. Chason, S. T. Picraux, J. M. Poate, J. O. Borland, M. I. Current, T. D. de le Rubia, D. J. Eaglesham, O. W. Holland, M. E. Law, C. W. Magee, J. W. Mayer, and A. F. Tasch, *J. Appl. Phys.* **81**, 6513 (1997).
- ²J. S. Williams, R. G. Elliman, M. C. Ridgway, C. Jagadish, S. L. Ellingboe, R. Goldberg, M. Petravic, W. C. Wong, Z. Dezhang, E. Nygren, and B. G. Svensson, *Nucl. Instrum. Methods Phys. Res. B* **80/81**, 507 (1993).
- ³J. O. Borland and R. Koelsch, *Solid State Technol.* **36**, 28 (1993).
- ⁴J. W. Corbett, J. P. Karins, and T. Y. Tan, *Nucl. Instrum. Methods* **182/183**, 457 (1981).
- ⁵B. G. Svensson, B. Mohadjeri, A. Hallen, J. H. Svensson, and J. W. Corbett, *Phys. Rev. B* **43**, 2292 (1991).
- ⁶K. S. Jones, S. Prussin, and E. R. Weber, *Appl. Phys. A: Solids Surf.* **45**, 1 (1988).
- ⁷P. A. Stolk, H.-J. Gossmann, D. J. Eaglesham, D. C. Jacobson, C. S. Rafferty, G. H. Golmer, M. Jaraiz, J. M. Poate, H. S. Luftman, and T. E. Haynes, *J. Appl. Phys.* **81**, 6031 (1997).
- ⁸A. Polman, *J. Appl. Phys.* **82**, R1 (1997).
- ⁹M. Jaraiz, G. H. Gilmer, J. M. Poate, and T. D. de le Rubia, *Appl. Phys. Lett.* **68**, 409 (1996).
- ¹⁰T. Motooka, S. Harada, and M. Ishimaru, *Phys. Rev. Lett.* **78**, 2980 (1997).
- ¹¹J. L. Benton, S. Libertino, P. Kringhøj, D. J. Eaglesham, J. M. Poate, and S. Coffa, *J. Appl. Phys.* **82**, 120 (1997).
- ¹²S. Coffa, F. Priolo, and A. Battaglia, *Phys. Rev. Lett.* **70**, 3756 (1993).

- ¹³S. Coffa, V. Privitera, F. Priolo, S. Libertino, and G. Mannino, *J. Appl. Phys.* **81**, 1639 (1997).
- ¹⁴V. Privitera, S. Coffa, F. Priolo, K. K. Larsen, and G. Mannino, *Appl. Phys. Lett.* **68**, 3422 (1996).
- ¹⁵A. Claveri, C. Vieu, J. Faure, and J. Beauvillain, *J. Appl. Phys.* **64**, 4415 (1988).
- ¹⁶S. Agarwal, Y. N. Mohapatra, and V. A. Singh, *J. Appl. Phys.* **77**, 3155 (1995).
- ¹⁷P. K. Giri and Y. N. Mohapatra, *J. Appl. Phys.* **78**, 262 (1995).
- ¹⁸S. Agarwal, Y. N. Mohapatra, V. A. Singh, and R. Sharan, *J. Appl. Phys.* **77**, 5725 (1995).
- ¹⁹P. K. Giri, S. Dhar, V. N. Kulkarni, and Y. N. Mohapatra, *J. Appl. Phys.* **81**, 260 (1997).
- ²⁰G. Goto, S. Yanagisawa, O. Wada, and H. Takanashi, *Appl. Phys. Lett.* **23**, 150 (1973).
- ²¹L. C. Kimerling, *J. Appl. Phys.* **45**, 1839 (1974).
- ²²M. Schulz, *Appl. Phys. Lett.* **23**, 31 (1973).
- ²³J. F. Zeigler, J. P. Biersack, and U. Littmark, *The Stopping of Ions in Solids* (Pergamon, New York, 1985).
- ²⁴J. Bollman and H. A. Klose, *Solid State Phenom.* **6&7**, 461 (1989).
- ²⁵V. Raineri, G. Fallica, and S. Libertino, *J. Appl. Phys.* **79**, 9012 (1996).
- ²⁶C. H. Seager, S. M. Myers, R. A. Anderson, W. L. Warren, and D. M. Follstaedt, *Phys. Rev. B* **50**, 2458 (1994).
- ²⁷R. K. Gupta, M. Tech. thesis, IIT Kanpur, India (1997).
- ²⁸A. Singh, *Solid-State Electron.* **28**, 223 (1985).
- ²⁹S. J. Fonash, *J. Appl. Phys.* **54**, 1966 (1983).
- ³⁰J. D. Willey and G. L. Miller, *IEEE Trans. Electron Devices* **ED-22**, 265 (1975).
- ³¹M. A. Lampert and P. Mark, *Current Injection in Solids* (Academic, New York, 1970).
- ³²A. Golan, R. Fastow, and M. Eizenberg, *J. Appl. Phys.* **67**, 1940 (1990).
- ³³J. E. Ejimania, *Solid-State Electron.* **29**, 841 (1986).
- ³⁴S. Nespurek and J. Sworakowski, *J. Appl. Phys.* **51**, 2098 (1980).
- ³⁵J. R. Troxell, *Solid-State Electron.* **26**, 539 (1983).
- ³⁶L. Palmetshofer and J. Reisinger, *J. Appl. Phys.* **72**, 2167 (1992).
- ³⁷P. K. Giri and Y. N. Mohapatra, *Appl. Phys. Lett.* **71**, 1682 (1997).
- ³⁸J. Bourgoin and M. Lanoo, in *Point Defects in Semiconductors II* (Springer, Berlin, 1983), p. 196.
- ³⁹Note that these experiments were done with low fluences and low-energy ions and clustering is not expected to limit the range of migration in this case.
- ⁴⁰K. K. Larsen, V. Privitera, S. Coffa, F. Priolo, S. U. Campisano, and A. Carnera, *Phys. Rev. Lett.* **76**, 1493 (1996).